AMOC Stability Amid Tipping Ice Sheets: The Crucial Role of Rate and Noise

Sacha Sinet[1,2], Peter Ashwin[3], Anna S. von der Heydt[1,2], and Henk A. Dijkstra[1,2]

[1]Department of Physics, Institute for Marine and Atmospheric research Utrecht, Utrecht University, Utrecht, The Netherlands
[2]Center for Complex Systems Studies, Utrecht University, Utrecht, The Netherlands
[3]Department of Mathematics and Statistics, University of Exeter, Exeter EX4 4QF, UK

Correspondence: Sacha Sinet (s.a.m.sinet@uu.nl)

Abstract. The Atlantic Meridional Overturning Circulation (AMOC) has reccently been categorised as core tipping element, for it is believed to be prone to critical transition under climate change, implying drastic consequences on a planetary scale. Moreover, the AMOC is strongly coupled to polar ice sheets via meltwater fluxes. On one hand, most studies agree on the fact that a collapse of the Greenland ice sheet would result in a weakening of AMOC. On the other hand, the consequences of a
5   collapse of the West Antarctica ice sheet are less well understood. However, some studies suggest that meltwater originating from the Southern Hemisphere is able to stabilize the AMOC. Using a conceptual model of the AMOC and a minimal parameterization of ice sheet collapse, we investigate the origin and relevance of this stabilization effect in both the deterministic and stochastic cases. While a substantial stabilization is found in both cases, we find that important rate and noise-induced effects result in bifurcation-induced tipping approaches to be inaccurate for predicting the AMOC stability.

1   Introduction

Several components of the Earth system might abruptly and/or irreversibly collapse under climate warming. Those are known as tipping elements (Lenton et al., 2008), each associated to a tipping point - a critical value of forcing above which the system is going to collapse. In a recent assessment, Armstrong McKay et al. (2022) classified the Atlantic Meridional Ocean Circulation (AMOC), the Greenland Ice Sheet (GIS) and West Antarctica Ice Sheet (WAIS) as global core tipping elements,
15   as the loss of any of those climate components would lead to severe consequences on a planetary scale. There, it was also suggested that those three tipping elements might be at risk within the Paris agreement warming range, while both polar ice sheets might already have crossed their critical threshold of global warming. Furthermore, an ongoing destabilization is in general supported by observations (see Caesar et al. (2018) for the AMOC, Shepherd et al. (2018) for the WAIS and Shepherd et al. (2020) for the GIS) or studies based on early warning signals (see Boers (2021), Michel et al. (2022) and Ditlevsen and
20   Ditlevsen (2023) for the AMOC, and Boers and Rypdal (2021) for the GIS).

From a theoretical standpoint, tipping events are most often understood as the expression of a dynamic bifurcation intrinsic to the system. In this case, bifurcation-induced tipping can be avoided ensuring that external drivers (typically the global temperature) do not cross the critical value at which the bifurcation takes place. However, tipping events can also occur via inherently different processes, as described by Ashwin et al. (2012). On one hand, those tipping events can be induced without

25   crossing any critical value of external forcing and, in fact, without the presence of any bifurcation. Such tipping phenomena typically occur when the rate of variation of external drivers is faster than the rate at which the system relaxes back to its attractor. The potential impact of those rate-induced tipping phenomena on the AMOC stability has been pointed out by numerous studies involving conceptual (Alkhayuon et al., 2019; Ritchie et al., 2023; Klose et al., 2023) or global ocean models (Lohmann and Ditlevsen, 2021). On the other hand, a tipping event can be triggered by the presence of stochastic

30   noise, routinely used to represent the unresolved variability of processes acting on a shorter timescale (Hasselmann, 1976; Frankignoul and Hasselmann, 1977). In this case, a system can collapse before crossing any critical value of forcing, solely due to the noise. In fact, noise-induced tipping phenomena potentially explain abrupt transitions observed in paleoclimatic records known as Dansgaard-Oeschger events (Ditlevsen et al., 2007; Ditlevsen and Johnsen, 2010). The impact of noise on the AMOC stability has been investigated in a conceptual model by Castellana et al. (2019). There, the variability associated

35   to the gradient of freshwater forcing over the Atlantic Ocean is able to induce a collapse of the overturning within the next century, with a probability estimated at about 15%. In a later study, similar noise-induced tipping events have been shown to also occur in an ensemble of CMIP5 models [Castellana and Dijkstra (2020)].

As a further complication, the study of each tipping element individually might not suffice for producing reliable projections of tipping behaviour. Indeed, those elements are not isolated but may interact with each other, sometimes strongly, making it

40   harder to predict the occurrence and severity of a tipping event. Arguably, the AMOC, GIS and WAIS form the most prominent example of such a coupled system of tipping elements. All three interact through various processes and on different timescales (Wunderling et al., 2021, 2023). On one hand, a GIS collapse and the associated release of meltwater into the northern Atlantic Ocean is known to imply, at best, a weakening of the AMOC (Jackson and Wood, 2018; Bakker et al., 2016). On the other hand, a collapse of the AMOC could imply a warming of the Southern Hemisphere (Jackson et al., 2015; Stouffer et al., 2006),

45   thereby accelerating ice loss in the WAIS (Favier et al., 2019; Joughin et al., 2014). Such chain of destabilizing events are often referred to as cascading tipping, or domino effect (Dekker et al., 2018; Klose et al., 2021; Wunderling et al., 2021). However, this coupled system might also contain some stabilizing feedback. In this case, the collapse of one component may stabilize others, thereby making a global cascading event less likely. For example, using the state-of-the-art climate model HadGEM3, the collapse of the AMOC has been shown to imply a cooling of typically 5 to 8°C over Greenland (Jackson et al., 2015),

50   which would inhibit ice loss of the GIS.

A substantial source of uncertainty in how a cascading tipping event could occur lies in how a sudden ice loss from the WAIS would impact the AMOC. There, many different processes are at play and might either tend to destabilize it or keep it from collapsing (Swingedouw et al., 2009; Berk et al., 2021). In a conceptual model representing the AMOC and both polar ice sheets, Sinet et al. (2023) recently showed that the WAIS meltwater flux is able to prevent an AMOC collapse against the

55   destabilization caused by both climate warming and ice loss from the GIS. The occurrence of an AMOC collapse drastically depends on the rate of forcing, as well as on the time delay between the tipping of both ice sheets. However, in this study, rate-induced effects were not explored in detail, and the stochastic case was not considered.

Motivated by the WAIS induced stabilization effect on the AMOC found by Sinet et al. (2023), we explore its relevance in a more comprehensive conceptual model of the AMOC, considering also the stochastic case. For this, we perform a variety of

60 model simulations using a simplified representation of tipping ice sheets. We aim to identify the distinct roles of rate, noise and bifurcation-induced effects. The experimental setup is presented in section 2. In section 3, we reproduce a set of model simulations similar to Sinet et al. (2023), yielding a qualitatively similar AMOC stabilization effect of the WAIS meltwater flux. In section 4, the bifurcation structure of the model is presented, allowing us to identify the presence of rate-induced effects. The robustness of this stabilization effect in the stochastic case is investigated in section 5. Finally, a summary and a

65 discussion are provided in section 6.

2 AMOC Model and Parameterized Ice Sheet Collapse

In this section, we describe the conceptual model used to represent the AMOC, and introduce a minimal representation of meltwater fluxes originating from the collapse of the GIS and WAIS.

a. Representation of the AMOC Model

b. Representative Meltwater Flux Trajectories
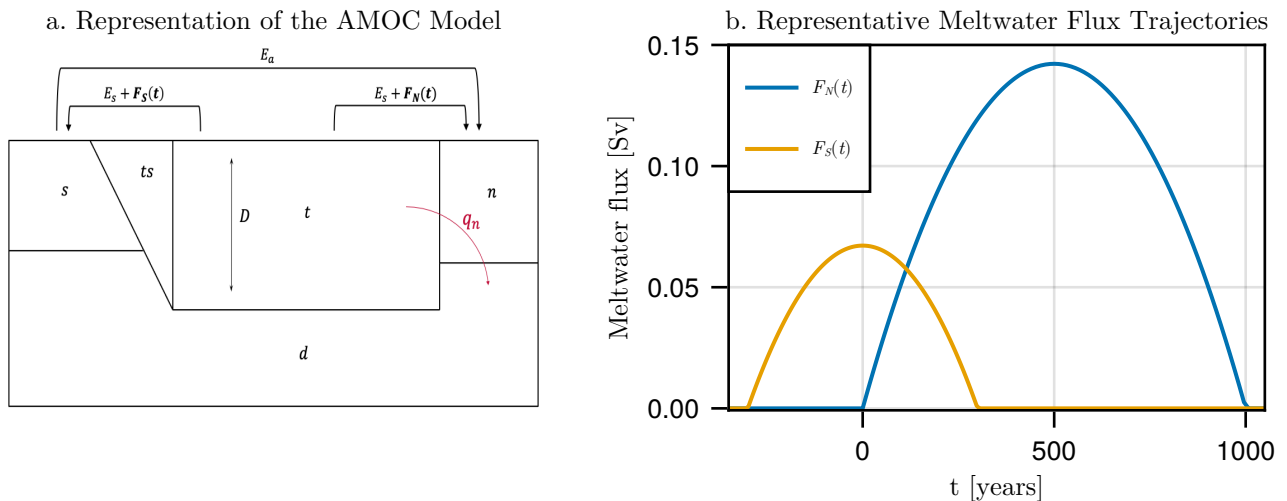
Figure 1. *(a) The AMOC dynamics is captured by water transport between five distinct boxes, namely the Southern Ocean box s, two thermocline boxes t and ts, a deep ocean box d and the northern Atlantic box n. Each individual salinity is allowed to vary, as well as the pycnocline depth D. The parameters E_a and E_s, denoting the asymmetric and symmetric component of the surface freshwater flux respectively, are chosen to initialise the AMOC in an ON state (i.e. with strictly positive overturning strength q_n). Meltwater fluxes $F_{N,S}(t)$ are added to the northern and southern box respectively, and compensated for via evaporation at the equator. (b) Representative trajectory of meltwater fluxes $F_{N,S}(t)$ as given by the set of equations (1)-(2) (or equations (1)-(3)). There, the collapse time of the GIS and WAIS is fixed to $P_N = 1000$ years and $P_S = 600$ years, and the tipping delay is fixed to $\Delta t = -300$ years (or the delay between the maxima of $F_N(t)$ and $F_S(t)$ to $\Delta t_{max} = -500$ years).*

70   The AMOC is represented using the model introduced by Cimatoribus et al. (2014). There, the Atlantic Ocean is divided into five different regions depicted by boxes having distinct salinities, whose volumes are allowed to vary depending on the pycnocline depth D (see Fig. 1.a). Furthermore, the model is forced via two surface freshwater fluxes E_s and E_a. The former stands for the amount of evaporation occurring in the tropical region and equally redistributed to each pole, while the latter introduces a pole-to-pole gradient of freshwater forcing. Given a value of E_s, Cimatoribus et al. (2014) have shown that this

75   model can yield bistability within some interval of E_a. Within this interval, one branch of stable steady states corresponds to a present-day-like AMOC with downwelling of dense waters in the northern box ($q_n > 0$), while the other corresponds to a ceased overturning ($q_n = 0$). Hereafter, we call those respectively ON and OFF state. For a more detailed description of the AMOC model, see Appendix A.

    To mimic the meltwater flux originating from collapsing ice sheets, time-dependent meltwater fluxes $F_{N,S}(t)$ are inserted

80   in the northern and southern box respectively, and compensated for via evaporation at the equator (see Fig. 1.a). Those are assumed to yield a parabolic shape in time (Fig. 1.b), as follows,

$$
F_N(t; P_N) = \begin{cases} -\dfrac{6V_N}{P_N^3} t(t - P_N) & \text{if } 0 < t < P_N, \\ 0 & \text{otherwise,} \end{cases}
\tag{1}
$$

$$
F_S(t; P_S, \Delta t) = \begin{cases} -\dfrac{1}{4}\dfrac{6V_S}{P_S^3}(t - \Delta t)(t - \Delta t - P_S) & \text{if } 0 < t - \Delta t < P_S, \\ 0 & \text{otherwise,} \end{cases}
\tag{2}
$$

85   where $P_{N,S}$ is the duration of the GIS and WAIS collapse, respectively. Given that the GIS collapse is always initiated at $t = 0$, the parameter Δt is the time (in years) at which the WAIS collapse is initiated, or the time delay between the initiation of those two tipping events (which can be both positive or negative). Also, the parameters $V_N = 2.99 \times 10^{15}$ m^3 and $V_S = 3.39 \times 10^{15}$ m^3 are the volumes of respectively the GIS and WAIS (as in Sinet et al. (2023), based on Morlighem et al. (2017, 2020)), resulting in the forcing (1)-(2) to conceptually capture a full collapse of both ice sheets. An alternative representation of $F_S(t)$

90   will also be used, where the tipping delay Δt is replaced by the delay between the maxima of both metlwater fluxes given by $\Delta t_{\max} = \Delta t + \frac{P_S - P_N}{2}$, which is positive if the maximum of $F_S(t)$ occurs after the maximum of $F_N(t)$. In this case, equation (2) is replaced by

$$
F_S(t; P_S, \Delta t_{\max}) = \begin{cases} -\dfrac{1}{4}\dfrac{6V_S}{P_S^3}\left(t - \Delta t_{\max} + \dfrac{P_S - P_N}{2}\right)\left(t - \Delta t_{\max} - \dfrac{P_S + P_N}{2}\right) & \text{if } 0 < t - \Delta t_{\max} + \dfrac{P_S - P_N}{2} < P_S, \\ 0 & \text{otherwise.} \end{cases}
\tag{3}
$$

    As an illustration of these two parametrizations of $F_S(t)$, the ice sheet tipping scenario represented in Fig. 1.b corresponds

95   to $\Delta t = -300$ years in (2), or equivalently $\Delta t_{\max} = -500$ years in (3). Finally, to account for the WAIS meltwater lost in the Pacific or Indian Oceans, we consider only a quarter of the meltwater originating from the WAIS to reach the Atlantic Ocean, as in Sinet et al. (2023).

3 Deterministic Regime

In this section, we perform a set of model simulations to highlight the existence of a stabilizing impact of WAIS meltwater
100 fluxes on the AMOC. For this, we initialise the AMOC in an ON state, choosing $E_a = 0.31$ Sv. First, we investigate the
situation in which only meltwater originating from the GIS is introduced in the Atlantic Ocean. In this case, the forcing is
given by equation (1) alone and is fully determined by the parameter P_N. We find that for $P_N \leq 1284$ years, the AMOC
ends in an OFF state. In the critical case $P_N = 1284$ years, the OFF state is reached at about year 850 as the meltwater flux
from the GIS amounts to approximately 0.1 Sv, consistent with typical forcing values leading the AMOC to a weak state in
105 comprehensive models (Jackson and Wood, 2018).

To check whether stabilization effects associated to WAIS meltwater fluxes exist in this model, we force the AMOC with
meltwater from both ice sheets. For this, we fix $P_N = 1000$ years in equation (1) such that, by virtue of the previous experiment,
the GIS forcing alone is sure to drive the AMOC to collapse. Indeed, using this value of P_N, the OFF state is reached at about
year 330 and the meltwater flux from the GIS reaches a maximal value of 0.14 Sv. We note that this value of P_N corresponds
110 to the lowest plausible GIS tipping duration proposed by Armstrong McKay et al. (2022), such that this GIS tipping event can
be thought of as a worst case scenario. Now, the WAIS melting trajectory is fully determined by either $(\Delta t, P_S)$ via equation
(2) or $(\Delta t_{\max}, P_S)$ via equation (3). Here and in the remainder of this document, we consider the range $P_S = [50, 5000]$ years,
encompassing about the lower half of the WAIS tipping duration interval proposed by Armstrong McKay et al. (2022). The
result of experiments involving meltwater fluxes from both ice sheets is represented in Fig. 2.a in the $(\Delta t, P_S)$ parameter space
115 and in Fig. 2.b in the $(\Delta t_{\max}, P_S)$ parameter space. We find a closed region in which the AMOC remains in an ON state (inside
the dark blue boundary), hereafter called the no-tipping region, while an OFF state was reached everywhere else (outside of
the dark blue boundary).

The existence of a no-tipping region can be understood as explained in Cimatoribus et al. (2014). Namely, given the sense
of the circulation, meltwater inserted into the southern box implies a freshening of the box ts (see Fig. 1.a). This results in an
120 increase of the density gradient between box ts and box n, and hence an increase of the overturning strength q_n (see appendix
A). However, on Fig. 2.a, there appears to be an upper limit of tipping delay at $\Delta t = 320$ years above which no stabilization
can takes place. Indeed, if no meltwater flux from the WAIS has already been applied by this time, the AMOC is already
engaged in its collapse. Also, the overall shape of the no-tipping region indicates that, to result in an efficient stabilization of
the AMOC, a longer WAIS collapse has to happen earlier than a shorter one. Although in a different experimental setup, these
125 results qualitatively agree with those in Sinet et al. (2023). In both Fig. 2.a and 2.b, there is an upper limit of WAIS tipping
duration at $P_S = 1600$ years, above which $F_S(t)$ does not reach sufficiently high values to compensate for the comparatively
strong GIS meltwater flux. Finally, in Fig. 2.b, the approximate symmetry of the no-tipping region suggests the existence of
a negative optimal value of $\Delta t_{\max} \approx 150$ years. This value is optimal in the sense that the range of P_S values for which a
stabilization occurs shrinks as $\Delta t_{\max}$ moves away from it, until the border of the no-tipping region is reached. In other words,
130 stabilization is most likely if the maximum of the WAIS meltwater flux occurs about 150 years before the maximum of the GIS
meltwater flux.
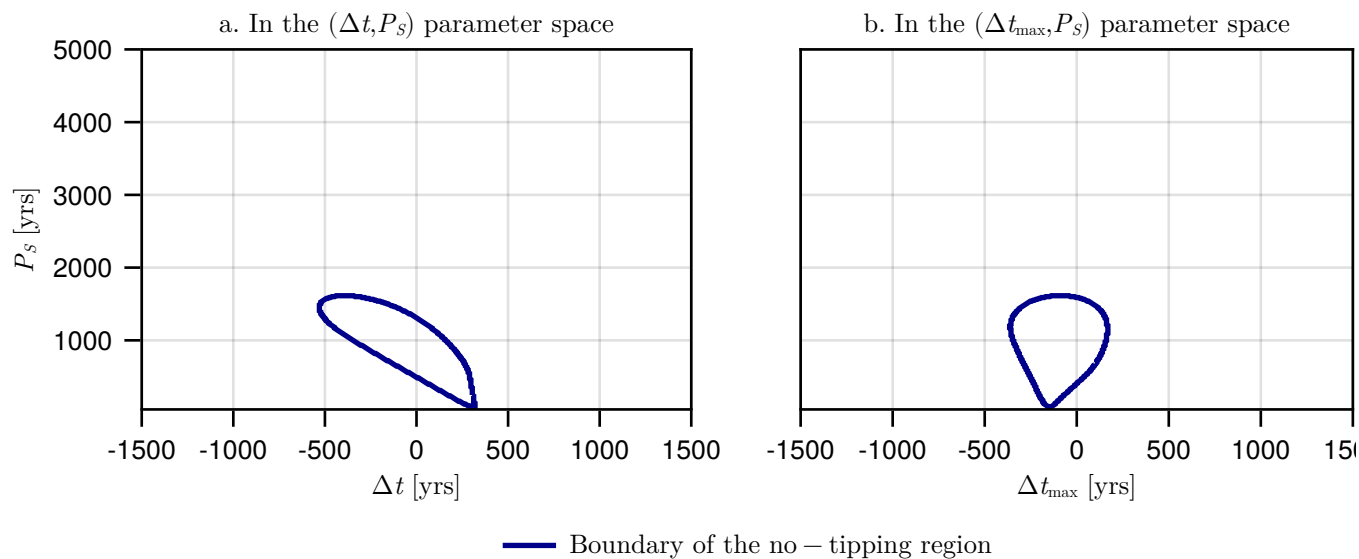
Figure 2. *Boundary of the no-tipping region in deterministic experiments involving both ice sheets, where the duration of the GIS collapse is fixed to $P_N = 1000$ years. Those are shown in (a) the $(\Delta t, P_S)$ parameter space and (b) the $(\Delta t_{max}, P_S)$ parameter space. All parameter configurations within the no-tipping region (dark blue curve) preserve the AMOC in an ON state ($q_n > 0$), while those outside lead the AMOC to an OFF state ($q_n = 0$).*

4   Bifurcation Structure and Rate Induced Effects

To gain a better understanding of the stabilization effect found in Fig. 2, we inspect the bifurcation structure of the AMOC model computed via numerical continuation (Veltz, 2020). On Fig. 3.a, steady states of the model are shown in terms of the
135   overturning strength q_n versus positive values of the meltwater flux in the northern box F_N. Those have been computed for three different values of $F_S = 0$, 0.04 and 0.08 Sv, yielding three distinct curves (with F_S increasing from darker to lighter). In each case, bistability is observed within some interval of F_N above which the branch of stable present-day-like AMOC ceases to exist, while the collapsed AMOC configuration ($q_n = 0$) is always stable. This is sufficient to infer the existence of a bifurcation-induced tipping point, implying the potential of a critical transition as F_N exceeds it. We note the presence of
140   Hopf bifurcations which move along the unstable branch as F_S increases, and a Bogdanov-Takens bifurcation creating a new Hopf bifurcation on the stable branch, which keeps close to the saddle-node bifurcation observed for each value of F_S (see Fig. 3.b). However, in terms of how the southern meltwater flux impacts the stability landscape, the most important general feature observed here is the expansion of the bistable region to higher values of F_N when F_S increases. This can in principle explain the stabilization effect taking place in previous experiments, as the tipping point of the AMOC becomes harder to reach.
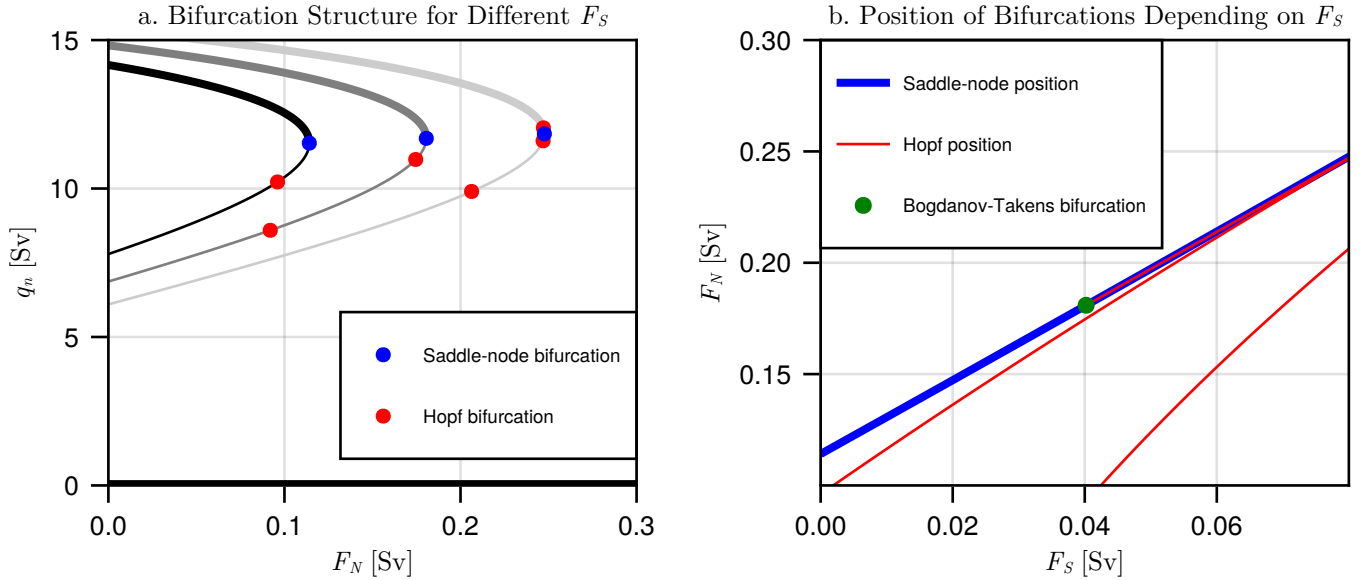
Figure 3. *(a) Bifurcation structure of the AMOC model in the (q_n, F_N) space. Thicker branches stand for stable steady states, while thinner branches indicate unstable steady states and bifurcations are denoted by coloured points. The bifurcation structure has been computed for three different values of $F_S = 0.0, 0.04$ and 0.08 (darker to lighter) . (b) Displacement of bifurcations as F_S varies. To the right of the Bogdanov-Takens bifurcation (green), a new Hopf bifurcation is created (in red, superposed to the saddle-node bifurcation).*

The value of F_N at which the bistable region ends is approximately proportional to F_S, with a proportionality coefficient δ approximately given by 1.68 (Fig. 3.b). Noting that in the case where $F_S = 0.00$ Sv, the bistable region ends at $F_{N,c} \approx 0.11$ Sv, it is possible to identify meltwater flux trajectories that never lead the AMOC outside of its bistable region. Namely, those satisfy

$$F_N(t) - \delta F_S(t) < F_{N,c}, \tag{4}$$

for all $t \in \mathbb{R}$. Given a fixed value of P_N, these form a closed and compact region in the $(\Delta t, P_S)$ and $(\Delta t_{max}, P_S)$ parameter space, for which the mathematical expression is given in appendix B. Hence, fixing $P_N = 1000$ years as in the experiment represented in Fig. 2, we can identify all parameter values for which no tipping point is ever overshot, hereafter called the no-overshoot region. In Fig. 4.a-b, the limits of the no-overshoot region are drawn in red, and the boundary of the no-tipping region found in Fig. 2 is drawn in dark blue. We find that these regions do not coincide, meaning that the AMOC stability cannot be predicted based on its bifurcation structure. Especially, we find that a collapse of the AMOC can happen inside the no-overshoot region (for parameter configurations within the red contour but outside of the dark blue contour). In this case, the AMOC reaches an OFF state without ever leaving its bistable region. Also, we find that an AMOC tipping can be avoided even in some cases where the tipping point is overshot (for parameter configurations within the dark blue contour but outside

of the red contour), a phenomena known as safe overshoot (Ritchie et al., 2021). Those are rate-induced effects, resulting in

160   rate-induced tipping (Ashwin et al., 2012) or tipping avoidance (Ritchie et al., 2023), respectively.
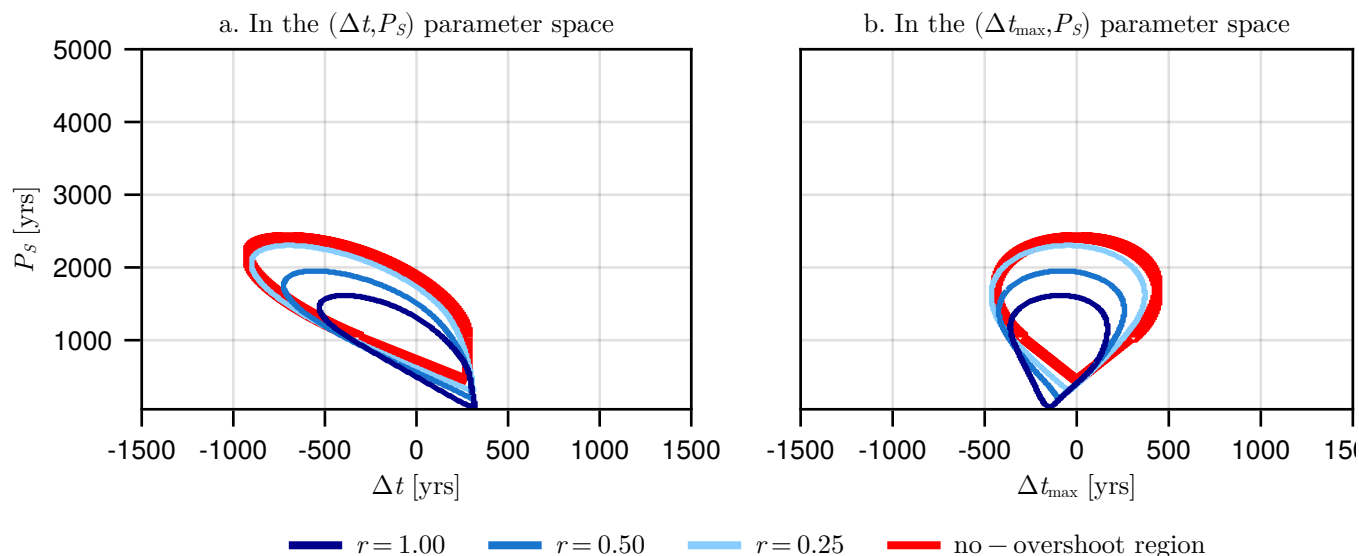
Figure 4. *Boundary of the no-overshoot region (in red) and the no-tipping region computed for different values of the rate parameter r (nuances of blue), drawn in (a) the $(\Delta t, P_S)$ parameter space and (b) the $(\Delta t_{max}, P_S)$ parameter space. The darker blue contour ($r = 1$) is the same as the one presented in Fig. 2, while lighter blue contours correspond to lower values of $r = 0.50$ and 0.25.*

Rate-induced effects are less pronounced as the rate at which the forcing varies is decreased. This can be tested via artificially expanding the forcing timescale, using $F_{N,S}(rt)$ rather than $F_{N,S}(t)$ in the experiments. This has the effect of multiplying durations and delays by the inverse of the rate parameter r. In other words, the rate of variation of the forcing decreases as r decreases. For values of r lower than one, we stray away from reality as bigger volumes of meltwater are inserted in the

165   Atlantic Ocean, but the bifurcation structure of the AMOC model under constant forcing remains unchanged, as well as the shape of the no-overshoot region. In Fig. 4.a-b, we represent the boundary of the no-tipping region in the same experiment using $r = 0.50$ and 0.25 (lighter tones of blue). As expected, we find that the no-overshoot region (delimited by the red curve) gradually becomes a better approximation of the no-tipping region, translating into a suppression of rate-induced effects. This results in transitions that are more consistent with the bifurcation-induced tipping case. Finally, we explain the approximate

170   symmetry of the no-tipping region in the $(\Delta t_{max}, P_S)$ parameter space found in section 3. The no-overshoot region (bounded by the red curve in Fig. 4.b) is perfectly symmetric around $\Delta t_{max} = 0$, which can also be directly inferred from its mathematical expression (see appendix B). Hence, in the limit where r reaches zero, $\Delta t_{max} = 0$ is the optimal value to result in a stabilization.

While it is clear that the symmetry is broken as the value of r increases to one, the no-tipping region still preserves some degree of symmetry around some optimal, negative value of $\Delta t_{\max}$. In other words, the (negative) optimal value of $\Delta t_{\max}$ depends on the rate of forcing.

The importance of rate-induced effects in this model can be explained by the fact that trajectories are relatively slowly attracted to the stable attractor. As an illustration, we note that the previously found critical value of GIS tipping duration at $P_N = 1284$ years in section 3 does not result in an overshoot of the tipping point. In this case, performing the same simulation with decreased r results in the AMOC to never reach the OFF state (as shown on Fig. 5.a). This originates from the slow timescale induced by the dynamics of the pycnocline depth D. In fact, the decay time towards the stable equilibrium can be computed as the inverse of the least negative eigenvalue of the associated stable state which, as shown on Fig. 5.b, is always above 190 years. This slow timescale can be connected to the pycnocline depth by computing the associated eigenvector, in which we find that the direction corresponding to the variable D dominates the others by approximately a factor 100. This indicates that, for the values of P_N considered, the separation between the forcing timescale and the decay timescale toward stable equilibria (driven by the dynamics of the pycnocline depth) is not large enough to prevent rate-induced effects.
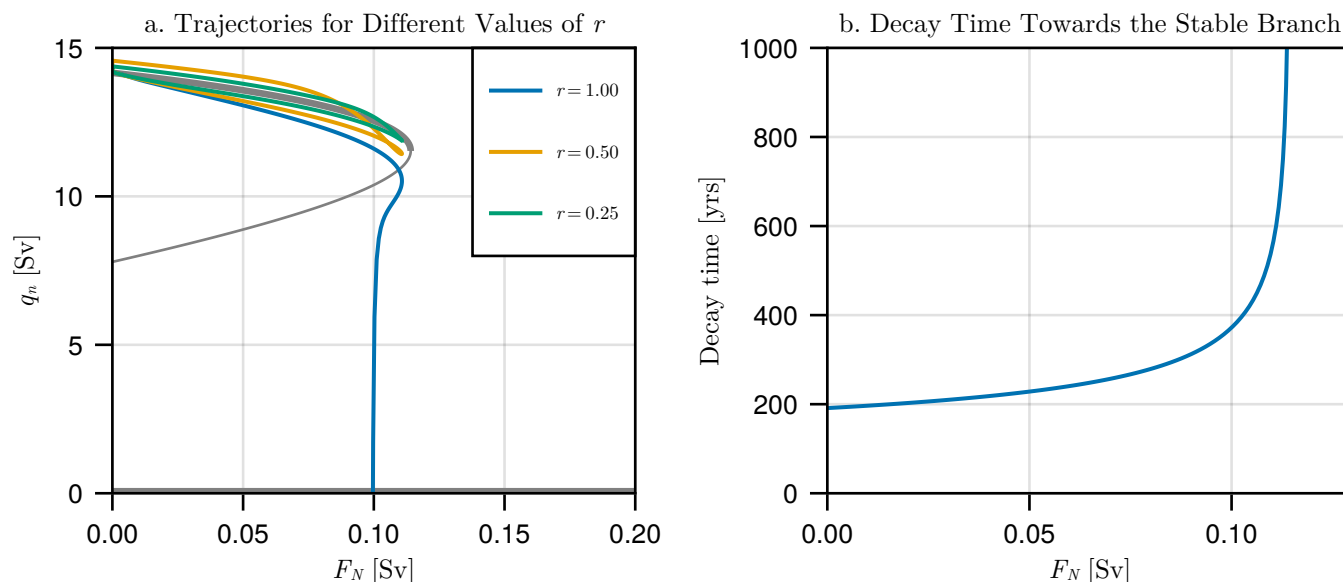
Figure 5. *(a) Trajectories in the experiment where only the GIS meltwater flux forces the AMOC via equation 1, using $P_N = 1284$ years and represented in the (q_n, F_N) space for different values of the rate parameter $r = 1.00$, 0.50 and 0.25. Steady states for fixed F_N are added in grey, where thicker lines stand for the stable states. (b) Variation of the decay time along the stable branch. The minimum is for $F_N = 0$ at about 190 years.*

5 Weak Noise Regime

In this section, we evaluate the relevance of the stabilization effect of WAIS meltwater fluxes on the AMOC when natural variability is added to the surface freshwater flux. To do so, we redefine the asymmetric component of the surface freshwater flux E_a in the following way (Castellana et al., 2019; Jacques-Dumas et al., 2023)

$$E_a(t) = \bar{E}_a(1 + f_\sigma \xi(t)). \tag{5}$$

Here, $\bar{E}_a$ is a constant representing the mean value of the asymmetric component of the surface freshwater flux, $\xi(t)$ is a white noise process with zero mean and unit variance, and f_σ is the noise strength parameter. As found by Castellana et al. (2019), a non-zero value of f_σ renders noise-induced tipping possible, where the AMOC can reach an OFF state solely due to the noise, independently of any meltwater forcing. From this point of view, both the cases in which the tipping point of the AMOC model can be overshot or not are relevant, and will be considered. To choose the noise strength parameter f_σ we note that, at the value $\bar{E}_a = 0.31$ (which we choose analogously to the deterministic case), Castellana et al. (2019) showed that $f_\sigma \in [0.1,\ 0.5]$ results in the AMOC reaching an OFF-state within 100 years with probability at least $1/3$. In our case, as we are interested in millennial timescales, such noise strengths would lead the AMOC to collapse almost surely regardless of the applied meltwater fluxes in any experiment. For a better signal-to-noise ratio, we choose to use a weaker noise by setting $f_\sigma = 0.05$. Finally, to be able to later compare transition probabilities in the same $(\Delta t, P_S)$ and $(\Delta t_{\max}, P_S)$ parameter spaces as before, we must ensure that white noise takes effect at the same given time in every simulation. Hence, we will systematically start numerical integration at year -3500, corresponding to the minimal time at which the WAIS tipping is initiated. In the remainder of this section, transition probabilities are computed via Monte-Carlo sampling using 10000 trajectories.

First, we focus on transition probabilities when only the GIS meltwater flux forces the AMOC via equation (1). This is performed for two distinct values of $P_N = 1000$ and 2000 years, where the former leads to an overshoot of the AMOC tipping point, while the latter does not. In Fig. 6, we show the time evolution of the cumulative transition probability $p_{\text{GIS}}(t)$, standing for the probability that the AMOC transitions to an OFF state before time t. We observe that before the GIS collapse ($t < 0$), this probability increases almost linearly in time, solely due to the noise. From the moment that the GIS collapse is initiated ($t = 0$), the probability sharply increases as the value of $F_N(t)$ brings the trajectory closer (or past) the border of the bistable region. This happens in both the cases where overshoot of the AMOC tipping point occurs or not although, in the case $P_N = 2000$ years, the probability increases at a milder rate than for $P_N = 1000$ years.

Second, using the same values of P_N, we force the AMOC model with the full forcing given by equations (1)-(2) (or equations (1)-(3)). Integrating the system in time, this leads to a new cumulative probability of AMOC transition $p_{\text{GIS,WAIS}}(t)$, interpreted in the same manner as $p_{\text{GIS}}(t)$. To assess the magnitude of any stabilization effect originating from the WAIS meltwater flux, we use the following metric:

$$\delta p(t) \equiv \frac{p_{\text{GIS,WAIS}}(t) - p_{\text{GIS}}(t)}{p_{\text{GIS}}(t)} * 100, \tag{6}$$
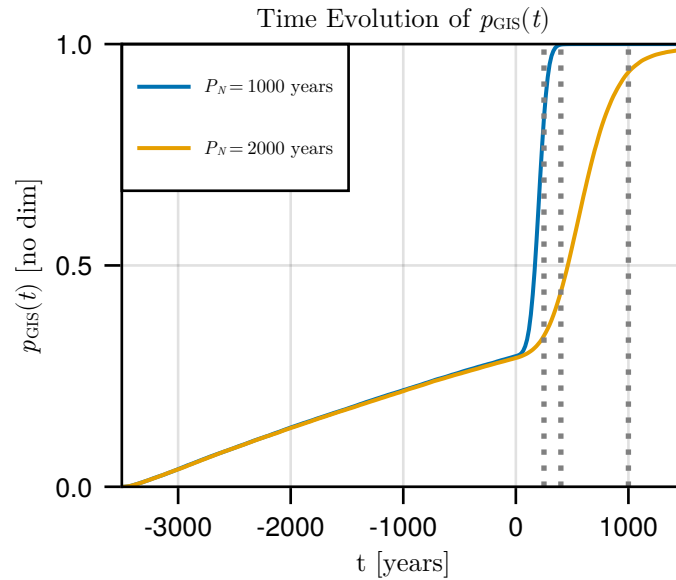
Figure 6. *Time evolution of the cumulative probability of AMOC transition $p_{GIS}(t)$ for $P_N = 1000$ (blue) and 2000 (yellow) years, using $f_\sigma = 0.05$ in both cases. Vertical dotted lines represent the three different times considered in Fig. 7. Probabilities were computed via Monte-Carlo sampling for 10000 trajectories.*

hereafter called relative probability change. It represents the percentage by which the cumulative transition probability varies with respect to the situation in which the GIS alone forces the AMOC. In other words, at any given time t, a negative value of $\delta p(t)$ indicates a stabilization induced by the WAIS collapse.

220   In Fig. 7.a, $P_N = 1000$ years was used, such that the AMOC tipping point is to be overshot everywhere except in the no-overshoot region (bounded by the red curve). The relative probability change is represented in both the $(\Delta t, P_S)$ parameter space (left column) and the $(\Delta t_{max}, P_S)$ parameter spaces (right column) at three different times, namely at year 250, 400 and 1000 (up to down, also drawn as dotted vertical lines on Fig. 6). At year 250, δp reaches -63%. While the overshoot of the AMOC tipping point has not occurred yet (and does not before year 280), it is interesting to note that the regions of

225 strongest probability decrease are consistent in shape with the no-overshoot region in both parameter spaces, although with a clear shift, which will be discussed at the end of this section. At year 400, only a small region of lower probability remains and gradually disappears as time increases, as can be seen at year 1000, where δp is uniformly close to zero. Results of the experiment using $P_N = 2000$ years, meaning that there is no region in the $(\Delta t, P_S)$ parameter space where the AMOC tipping point is ever overshot, is presented in Fig. 7.b. In this case, δp at year 250 is already substantially negative in a wide region of

230 the parameter space, and even more so at year 400. Importantly, we see that the stabilization is still present and substantial on longer timescales, as seen at year 1000. It is also interesting to note that the region of strongest probability decrease gradually becomes similar in shape to the previously found no-overshoot region as, here, no overshoot is ever to occur. However, as t increases, the center of this region clearly shifts toward higher values of Δt_{max}. This also happens in the case $P_N = 1000$

Figure 7. *Evolution of the relative probability change $\delta p(t)$ (defined by equation (6)) in stochastic experiments using $f_\sigma = 0.05$. We use (a) $P_N = 1000$ years, in which case the tipping point of the AMOC is overshot outside of the no-overshoot region (bounded by the red curve) and (b) $P_N = 2000$ years, in which case the tipping point of the AMOC is never overshot. For both (a) and (b), results are drawn in the $(\Delta t, P_S)$ parameter space (left column) and in the $(\Delta t_{max}, P_S)$ parameter space (right column) at three different times, namely $t = 250, 400$ and 1000 years (top to bottom). Each probability has been computed via Monte-Carlo sampling, using 10000 trajectories.*

years (Fig. 7.a), although less clearly. In summary, we find that the relative probability change can be substantially negative
in both the case when an AMOC overshoot can occur or not. However, varying the forcing rate yields important quantitative
differences in the magnitude of this stabilization effect, and on its specific timescale.

In Fig. 7.a, we found that the regions of strongest probability change and the no-overshoot region are similar in shape but
not in location. Analogously to the results of section 4, it is tempting to also relate this shift to rate-induced effects. This can
be verified by performing similar stochastic experiments for a lower value of the rate parameter r (used as in section 4). In
Fig. 8, we show the results obtained using $P_N = 1000$ years and $r = 0.25$. Again, to present results in the same $(\Delta t, P_S)$ and
$(\Delta t_{max}, P_S)$ parameter space, we ensure that the noise is added at the same time in all experiments by starting integration
at $t = -14000$ years. Hence, quantitative differences with respect to Fig. 7.a can be related to the fact that white noise acts
during a much longer time, while the region in which δp is most negative remains similar. Most importantly, we find that the
no-overshoot region does not become a better approximation of the region of strongest probability decrease at any time, despite
the low value used for the rate parameter r. This implies that the shift between the no-overshoot region and the region in which
δp is most negative cannot be explained (only) by rate-induced effects, but clearly involves noise-induced effects.

6   Summary and Discussion

In this study, the stability of the AMOC was explored in numerical simulations involving meltwater fluxes from both polar ice
sheets. Although in a different experimental setup, the same qualitative results of Sinet et al. (2023) were verified, where the
occurrence of an AMOC tipping depends on the timescale of both ice sheet collapses, and the delay between those collapses.
In a worst case scenario where the GIS fully collapses in 1000 years (as suggested by Armstrong McKay et al. (2022)),
deterministic results of section 3 indicated that a stabilizing influence of the WAIS collapse is strong enough to stabilize the
AMOC. Notably, this stabilization can occur for a relatively fast WAIS collapse lasting up to 1600 years, corresponding to
the lower projections of WAIS tipping durations (Armstrong McKay et al., 2022). Regarding the AMOC stabilization, the use
of two different parametrizations of WAIS tipping trajectories informed us on the existence of some optimal scenario for the
tipping of ice sheets, where the peak of WAIS meltwater flux occurs about 150 years before the peak of GIS meltwater flux.

In section 4, a detailed investigation of the AMOC bifurcation structure allowed to identify the no-overshoot region in the
forcing parameter space, defining WAIS tipping scenarios for which the tipping point of the AMOC is never reached. This
revealed that an AMOC collapse could be induced without leaving the bistable regime at any time, as well as the existence
of safe-overshoot trajectories. Such rate-induced effects occur when ice sheets collapse on a timescale which is comparable
to the recovery timescale of the AMOC, whose high value originates from the slow dynamics of the pycnocline depth. The
existence of those rate-indudced effects was confirmed by artificially slowing down the rate of variation of meltwater input,
yielding results that became more consistent with bifurcation-induced critical transitions. This analysis allows us to find that
the previously found optimal value of 150 years between the peaks of both meltwater fluxes is highly rate dependant.

Under stochastic noise in the surface freshwater flux (section 5), the stabilization effect of WAIS meltwater fluxes remains
important. In contrast to the determinstic context (section 3), a drastic decrease of the AMOC transition probability is now
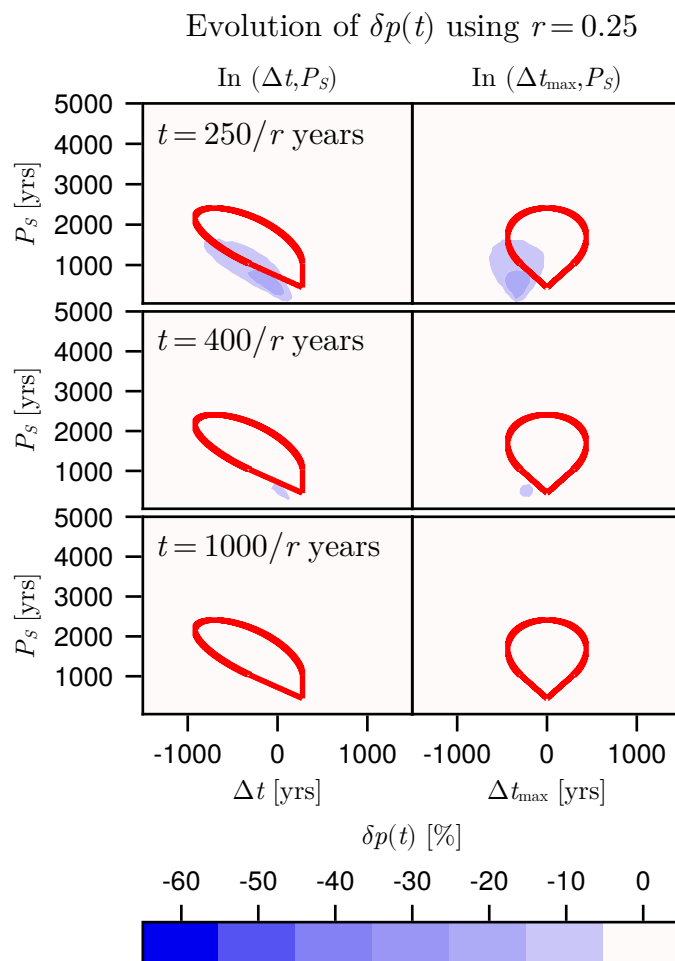
Figure 8. *Same as Fig. 7.a, using a lower value of the rate parameter $r = 0.25$. Also, the three values of t used in Fig. 7.a are here divided by the rate parameter r. Each probability has been computed via Monte-Carlo sampling using 10000 trajectories.*

possible in the case of slower WAIS collapse of up to 5000 years, spanning about the lower half of the range of WAIS tipping durations suggested by Armstrong McKay et al. (2022). On the one hand, we investigated the worst case scenario in which the GIS fully collapses in 1000 years, such that an overshoot of the AMOC tipping point can occur. In this case, we found that some WAIS trajectories result in a substantial decrease of the AMOC tipping probability (of up -63%), although remaining important only on the centennial timescale. On the other hand, we considered cases implying a comparatively slower GIS tipping lasting 2000 years, such that the tipping point of the AMOC is never overshot. In this case, we found that a similar probability decrease can persist way longer in time, on the millennial timescale. Finally, we were able to demonstrate that, due to noise-induced effects, ice sheet tipping scenarios yielding the strongest stabilization cannot be accurately predicted by

275 bifurcation analysis. Yet, similarities between the region of strongest stablization and the no-overshoot region motivates further investigation via the tools of stochastic dynamics (Berglund and Gentz, 2006).

Clearly, the scope of those results are limited by the conceptual nature of the model used, as was the case in Sinet et al. (2023). Indeed, important interactions and processes are ommited, and ice sheet melting trajectories were purposefully chosen to be minimalistic. A direct extension of this study would be to investigate how those results compare to those obtained in a

280 three-dimensional comprehensive global ocean model which, as in our case, can be obtained using only prescribed meltwater fluxes.

Nonetheless, the existence of such important rate and noise-induced effects at the conceptual level informs us on the limits of an analysis focused solely on bifurcation-induced transitions. It suggests that maintaining meltwater fluxes under some critical value might not suffice for ensuring the AMOC stability. Yet, the significant stabilizing impact of a WAIS collapse on the

285 AMOC stability as found in Sinet et al. (2023) is consistently found in a different conceptual AMOC model, and motivates further investigations. Finally, the decisive role of forcing rates encourages efforts to produce accurate predictions of ice sheet melting under future global warming.

Code availability. Julia codes used for producing the results and plots have been archived within the open access repository Zenodo (Sinet, 2023)

Appendix A: AMOC Box Model

290

The time evolution of salinities S_i for $i \in \{t, ts, n, s, d\}$ and the pycnocline depth D are given by differential equations identical to those used earlier (Cimatoribus et al., 2014; Castellana et al., 2019; Jacques-Dumas et al., 2023), except for the addition of time-dependent meltwater fluxes $F_{N,S}(t)$ defined by equations (1)-(2) (or equations (1)-(3)), as follows

$$\frac{\mathrm{d}\left(V_\mathrm{t} S_\mathrm{t}\right)}{\mathrm{d}t} = q_\mathrm{s}\left(\theta\left(q_\mathrm{s}\right)S_\mathrm{ts} + \theta\left(-q_\mathrm{s}\right)S_\mathrm{t}\right) + q_\mathrm{u}S_\mathrm{d} - \theta\left(q_\mathrm{n}\right)q_\mathrm{n}S_\mathrm{t} + r_\mathrm{s}\left(S_\mathrm{ts} - S_\mathrm{t}\right) + r_\mathrm{n}\left(S_\mathrm{n} - S_\mathrm{t}\right) + \left(2E_\mathrm{s} + F_N(t) + F_S(t)\right)S_0 \quad \text{(A1)}$$

295
$$\frac{\mathrm{d}\left(V_{t_\mathrm{s}} S_\mathrm{ts}\right)}{\mathrm{d}t} = q_\mathrm{Ek}S_\mathrm{s} - q_\mathrm{e}S_\mathrm{ts} - q_\mathrm{s}\left(\theta\left(q_\mathrm{s}\right)S_\mathrm{ts} + \theta\left(-q_\mathrm{s}\right)S_\mathrm{t}\right) + r_\mathrm{s}\left(S_\mathrm{t} - S_\mathrm{ts}\right) \quad \text{(A2)}$$

$$\frac{\mathrm{d}\left(V_\mathrm{n} S_\mathrm{n}\right)}{\mathrm{d}t} = \theta\left(q_\mathrm{n}\right)q_\mathrm{n}\left(S_\mathrm{t} - S_\mathrm{n}\right) + r_\mathrm{n}\left(S_\mathrm{t} - S_\mathrm{n}\right) - \left(E_\mathrm{s} + E_\mathrm{a} + F_N(t)\right)S_0 \quad \text{(A3)}$$

$$\frac{\mathrm{d}\left(V_\mathrm{s} S_\mathrm{s}\right)}{\mathrm{d}t} = q_\mathrm{s}\left(\theta\left(q_\mathrm{s}\right)S_\mathrm{d} + \theta\left(-q_\mathrm{s}\right)S_\mathrm{s}\right) + q_\mathrm{e}S_\mathrm{ts} - q_\mathrm{Ek}S_\mathrm{s} - \left(E_\mathrm{s} - E_\mathrm{a} + F_S(t)\right)S_0 \quad \text{(A4)}$$

$$\left(A + \frac{L_{x_A}L_y}{2}\right)\frac{\mathrm{d}D}{\mathrm{d}t} = q_\mathrm{u} + q_\mathrm{Ek} - q_\mathrm{e} - \theta\left(q_\mathrm{n}\right)q_\mathrm{n} \quad \text{(A5)}$$

$$S_0 V_0 = V_\mathrm{n}S_\mathrm{n} + V_\mathrm{d}S_\mathrm{d} + V_\mathrm{t}S_\mathrm{t} + V_\mathrm{ts}S_\mathrm{ts} + V_\mathrm{s}S_\mathrm{s}, \quad \text{(A6)}$$

300   where $\theta(x)$ stands for the Heaviside function. Those include wind driven transports $r_{s,n}$ originating from sub-tropical gyres, and the following volume transports

$$q_{\mathrm{Ek}} = \frac{\tau L_{xS}}{\rho_0 \left|f_S\right|} \tag{A7}$$

$$q_{\mathrm{e}} = A_{GM} \frac{L_{xA}}{L_y} D \tag{A8}$$

$$q_{\mathrm{s}} = q_{\mathrm{Ek}} - q_{\mathrm{e}} \tag{A9}$$

305
$$q_{\mathrm{n}} = \eta \frac{\rho_{\mathrm{n}} - \rho_{\mathrm{ts}}}{\rho_0} D^2 \tag{A10}$$

$$q_{\mathrm{u}} = \frac{\kappa A}{D}, \tag{A11}$$

where densities ρ_i for $i \in \{n, ts\}$ are given by

$$\rho_{\mathrm{i}} = \rho_0 \left(1 - \alpha \left(T_{\mathrm{i}} - T_0\right) + \beta \left(S_{\mathrm{i}} - S_0\right)\right), \tag{A12}$$

and volumes are given by

310
$$V_{\mathrm{t}} = AD \tag{A13}$$

$$V_{\mathrm{ts}} = \frac{L_{xA} L_y}{D} \tag{A14}$$

$$V_{\mathrm{d}} = V_0 - V_{\mathrm{t}} - V_{\mathrm{ts}} - V_{\mathrm{n}} - V_{\mathrm{s}}. \tag{A15}$$

The different constants used in the model are provided in Table A1.

Appendix B: No-Overshoot Zone

315   As justified in section 4, meltwater forcing trajectories will never bring the AMOC model outside of its bistable region if condition (4) is verified for all $t \in \mathbb{R}$. Given a set value of $P_N > 0$, such trajectories (if they exist) are found in the $(\Delta t, P_S)$ and $(\Delta t_{\max}, P_S)$ parameter spaces by analysis, yielding the no-overshoot region. In what follows, computations are performed in the $(\Delta t_{\max}, P_S)$ parameter space. We begin by noting that $F_N(t)$ overshoots the critical value $F_{N,c}$ if and only if

$$3V_N - 2P_N F_{N,c} > 0, \tag{B1}$$

320   without what condition (4) is trivially verified in all cases. In the case where (B1) holds, the overshoot occurs during the interval $]t_{o-}, t_{o+}[$, where

$$t_{o-} = -\frac{P_N^3}{6V_N} \sqrt{\frac{3V_N(3V_N - 2P_N F_{N,c})}{P_N^4}} + \frac{P_N}{2} \tag{B2}$$

and

$$t_{o+} = \frac{P_N^3}{6V_N} \sqrt{\frac{3V_N(3V_N - 2P_N F_{N,c})}{P_N^4}} + \frac{P_N}{2}. \tag{B3}$$

Table A1. Constants used for the AMOC model

Parameters of the AMOC model		
V_0	3×10^{17} m^3	Total volume of the basin
V_{n}	3×10^{15} m^3	Volume of the northern box
V_{S}	9×10^{15} m^3	Volume of the southern box
A	1×10^{14} m^2	Horizontal area of the Atlantic pycnocline
L_{xA}	1×10^7 m	Zonal extent of the Atlantic Ocean at its southern end
L_y	1×10^6 m	Meridional extent of the frontal region of the Southern Ocean
L_{xS}	3×10^7 m	Zonal extent of the Southern Ocean
τ	0.1Nm^{-2}	Average zonal wind stress amplitude
A_{GM}	1700 m^2 s^{-1}	Eddy diffusivity
f_S	-10^{-4} s^{-1}	Coriolis parameter
ρ_0	1027.5 kg m^{-3}	Reference density
κ	10^{-5} m^2 s^{-1}	Vertical diffusivity
S_0	35psu	Reference salinity
T_0	5 K	Reference temperature
T_{n}	5 K	Temperature of the northern box
T_{ts}	10 K	Temperature of the box "ts"
η	3×10^4 m s^{-1}	Hydraulic constant
α	2×10^{-4} K^{-1}	Thermal expansion coefficient
β	8×10^{-4}psu^{-1}	Haline contraction coefficient
r_{S}	1×10^7 m^3 s^{-1}	Transport by the southern subtropical gyre
r_{n}	5×10^6 m^3 s^{-1}	Transport by the northern subtropical gyre
E_{s}	0.17×10^6 m^3 s^{-1}	Symmetric freshwater flux

325 Now, by virtue of the positivity of $F_S(t)$, a necessary condition for condition (4) to be satisfied is that $F_S(t)$ does not vanish for any t in $]t_{o-}, t_{o+}[$. In other words, $]t_{o-}, t_{o+}[$ must be fully contained in $\left[\Delta t_{\max} - \frac{P_S - P_N}{2}, \Delta t_{\max} + \frac{P_S + P_N}{2}\right]$, which is true if and only if

$$|\Delta t_{\max}| \leq t_{o+} - \frac{P_S + P_N}{2}. \tag{B4}$$

In this case, it remains only to ensure that the second degree polynomial

330 $$G(t) = F_N(t) - \delta F_S(t) - F_{N,c} \tag{B5}$$

$$= -\frac{6V_N}{P_N^3} t(t - P_N) + \frac{\delta}{4} \frac{6V_S}{P_S^3} \left(t - \Delta t_{\max} + \frac{P_S - P_N}{2}\right) \left(t - \Delta t_{\max} - \frac{P_S + P_N}{2}\right) - F_{N,c} \tag{B6}$$

does not overshoot zero within the time interval interval $]t_{0-}, t_{0+}[$. Again, by virtue of the positivity of $F_S(t)$, this is true if and only if one of the three following criteria holds

    – $\frac{d^2G(t)}{dt^2}$ is always positive or zero. This implies that $G(t)$ is majored by zero within $]t_{0-}, t_{0+}[$, and is true if and only if

335
$$P_S \leq P_N \sqrt[3]{\frac{\delta V_S}{4V_N}};\tag{B7}$$

    – $\frac{d^2G(t)}{dt^2}$ is always strictly negative, but $G(t)$ does not overshoot zero for any value of t. It is true if and only if the discriminant of $G(t)$ is negative or zero, translating into

$$48P_S^4 V_N^2 + 3\delta^2 P_N^4 V_S^2 + 8\delta F_{N,c} P_N^4 P_S V_S + 48\delta P_N V_N P_S V_S \left(\Delta t_{\max}\right)^2$$
$$- 32F_{N,c} P_N V_N P_S^4 - 12\delta P_N^3 V_N P_S V_S - 12\delta P_N V_N P_S^3 V_S \leq 0 \tag{B8}$$

340
    – $\frac{d^2G(t)}{dt^2}$ is always strictly negative and $G(t)$ overshoots zero, but only in a finite region outside of $]t_{0-}, t_{0+}[$. This is equivalent to requiring that the maximum of $G(t)$ is found outside of $]t_{0-}, t_{0+}[$, which is true if and only if

$$2t_{o+} - P_N \leq 2\delta P_N^3 V_S \left| \frac{\Delta t_{\max}}{4V_N P_S^3 - \delta V_S P_N^3} \right|.\tag{B9}$$

To summary, given a set value of $P_N > 0$ for which $F_N(t)$ overshoots $F_{N,c}$ (meaning that condition (B1) holds), forcing trajectories verifying condition (4) may exist. Those verify (B4), along with either criteria (B7),(B8) or (B9). We note that, as
345 all those condition are invariant under the transformation $\Delta t_{\max} \rightarrow -\Delta t_{\max}$, the no-overshoot region yields an axial symmetry around $\Delta t_{\max} = 0$. Finally, this region can be described in the $(\Delta t, P_S)$ parameter space, simply by substituting $\Delta t = \Delta t_{\max} - \frac{P_S - P_N}{2}$ in each condition.

Author contributions. SS carried out the analysis and drafted the paper. PA, ASvdH and HAD advised on the study. All authors contributed to the submitted paper.

350 *Competing interests.* No competing interests are present.

Acknowledgements. This project has received funding from the European Union's Horizon 2020 research and innovation programme under the Marie Skłodowska-Curie Grant Agreement No. 956170 (CriticalEarth).

References

Alkhayuon, H., Ashwin, P., Jackson, L. C., Quinn, C., and Wood, R. A.: Basin bifurcations, oscillatory instability and rate-induced thresholds
for Atlantic meridional overturning circulation in a global oceanic box model, Proceedings of the Royal Society A: Mathematical, Physical
and Engineering Sciences, 475, 20190051, https://doi.org/10.1098/rspa.2019.0051, publisher: Royal Society, 2019.

Armstrong McKay, D. I., Staal, A., Abrams, J. F., Winkelmann, R., Sakschewski, B., Loriani, S., Fetzer, I., Cornell, S. E., Rock-
ström, J., and Lenton, T. M.: Exceeding 1.5°C global warming could trigger multiple climate tipping points, Science, 377, eabn7950,
https://doi.org/10.1126/science.abn7950, publisher: American Association for the Advancement of Science, 2022.

Ashwin, P., Wieczorek, S., Vitolo, R., and Cox, P.: Tipping points in open systems: bifurcation, noise-induced and rate-dependent examples
in the climate system, Philosophical Transactions of the Royal Society A: Mathematical, Physical and Engineering Sciences, 370, 1166–
1184, https://doi.org/10.1098/rsta.2011.0306, publisher: Royal Society, 2012.

Bakker, P., Schmittner, A., Lenaerts, J. T. M., Abe-Ouchi, A., Bi, D., van den Broeke, M. R., Chan, W.-L., Hu, A., Beadling, R. L.,
Marsland, S. J., Mernild, S. H., Saenko, O. A., Swingedouw, D., Sullivan, A., and Yin, J.: Fate of the Atlantic Meridional Overturn-
ing Circulation: Strong decline under continued warming and Greenland melting, Geophysical Research Letters, 43, 12,252–12,260,
https://doi.org/10.1002/2016GL070457, _eprint: https://onlinelibrary.wiley.com/doi/pdf/10.1002/2016GL070457, 2016.

Berglund, N. and Gentz, B.: Noise-Induced Phenomena in Slow-Fast Dynamical Systems: A Sample-Paths Approach, Probability and Its
Applications, Springer London, https://books.google.nl/books?id=c3w0z--7QJAC, 2006.

Berk, J. v. d., Drijfhout, S. S., and Hazeleger, W.: Circulation adjustment in the Arctic and Atlantic in response to Greenland and Antarctic
mass loss, Climate Dynamics, 57, 1689–1707, https://doi.org/10.1007/s00382-021-05755-3, 2021.

Boers, N.: Observation-based early-warning signals for a collapse of the Atlantic Meridional Overturning Circulation, Nature Climate
Change, 11, 680–688, https://doi.org/10.1038/s41558-021-01097-4, number: 8 Publisher: Nature Publishing Group, 2021.

Boers, N. and Rypdal, M.: Critical slowing down suggests that the western Greenland Ice Sheet is close to a tipping point, Proceedings of
the National Academy of Sciences, 118, e2024192118, https://doi.org/10.1073/pnas.2024192118, publisher: Proceedings of the National
Academy of Sciences, 2021.

Caesar, L., Rahmstorf, S., Robinson, A., Feulner, G., and Saba, V.: Observed fingerprint of a weakening Atlantic Ocean overturning circula-
tion, Nature, 556, 191–196, https://doi.org/10.1038/s41586-018-0006-5, number: 7700 Publisher: Nature Publishing Group, 2018.

Castellana, D. and Dijkstra, H. A.: Noise-induced transitions of the Atlantic Meridional Overturning Circulation in CMIP5 models, Scientific
Reports, 10, 20040, https://doi.org/10.1038/s41598-020-76930-5, number: 1 Publisher: Nature Publishing Group, 2020.

Castellana, D., Baars, S., Wubs, F. W., and Dijkstra, H. A.: Transition Probabilities of Noise-induced Transitions of the Atlantic Ocean
Circulation, Scientific Reports, 9, 20284, https://doi.org/10.1038/s41598-019-56435-6, number: 1 Publisher: Nature Publishing Group,
2019.

Cimatoribus, A. A., Drijfhout, S. S., and Dijkstra, H. A.: Meridional overturning circulation: stability and ocean feedbacks in a box model,
Climate Dynamics, 42, 311–328, https://doi.org/10.1007/s00382-012-1576-9, 2014.

Dekker, M. M., von der Heydt, A. S., and Dijkstra, H. A.: Cascading transitions in the climate system, Earth System Dynamics, 9, 1243–1260,
https://doi.org/10.5194/esd-9-1243-2018, publisher: Copernicus GmbH, 2018.

Ditlevsen, P. and Ditlevsen, S.: Warning of a forthcoming collapse of the Atlantic meridional overturning circulation, Nature Communica-
tions, 14, 4254, https://doi.org/10.1038/s41467-023-39810-w, 2023.

Ditlevsen, P. D. and Johnsen, S. J.: Tipping points: Early warning and wishful thinking, Geophysical Research Letters, 37,
390   https://doi.org/10.1029/2010GL044486, _eprint: https://onlinelibrary.wiley.com/doi/pdf/10.1029/2010GL044486, 2010.

Ditlevsen, P. D., Andersen, K. K., and Svensson, A.: The DO-climate events are probably noise induced: statistical investigation of the
claimed 1470 years cycle, Climate of the Past, 3, 129–134, https://doi.org/10.5194/cp-3-129-2007, publisher: Copernicus GmbH, 2007.

Favier, L., Jourdain, N. C., Jenkins, A., Merino, N., Durand, G., Gagliardini, O., Gillet-Chaulet, F., and Mathiot, P.: Assessment of sub-shelf
melting parameterisations using the ocean–ice-sheet coupled model NEMO(v3.6)–Elmer/Ice(v8.3), Geoscientific Model Development,
395   12, 2255–2283, https://doi.org/10.5194/gmd-12-2255-2019, publisher: Copernicus GmbH, 2019.

Frankignoul, C. and Hasselmann, K.: Stochastic climate models, Part II Application to sea-surface temperature anoma-
lies   and   thermocline   variability,   Tellus,   29,   289–305,   https://doi.org/10.1111/j.2153-3490.1977.tb00740.x,   _eprint:
https://onlinelibrary.wiley.com/doi/pdf/10.1111/j.2153-3490.1977.tb00740.x, 1977.

Hasselmann, K.: Stochastic climate models Part I. Theory, Tellus, 28, 473–485, https://doi.org/10.1111/j.2153-3490.1976.tb00696.x, _eprint:
400   https://onlinelibrary.wiley.com/doi/pdf/10.1111/j.2153-3490.1976.tb00696.x, 1976.

Jackson, L. C. and Wood, R. A.: Hysteresis and Resilience of the AMOC in an Eddy-Permitting GCM, Geophysical Research Letters, 45,
8547–8556, https://doi.org/10.1029/2018GL078104, _eprint: https://onlinelibrary.wiley.com/doi/pdf/10.1029/2018GL078104, 2018.

Jackson, L. C., Kahana, R., Graham, T., Ringer, M. A., Woollings, T., Mecking, J. V., and Wood, R. A.: Global and European climate impacts
of a slowdown of the AMOC in a high resolution GCM, Climate Dynamics, 45, 3299–3316, https://doi.org/10.1007/s00382-015-2540-2,
405   2015.

Jacques-Dumas, V., van Westen, R. M., Bouchet, F., and Dijkstra, H. A.: Data-driven methods to estimate the committor function in con-
ceptual ocean models, Nonlinear Processes in Geophysics, 30, 195–216, https://doi.org/10.5194/npg-30-195-2023, publisher: Copernicus
GmbH, 2023.

Joughin, I., Smith, B. E., and Medley, B.: Marine Ice Sheet Collapse Potentially Under Way for the Thwaites Glacier Basin, West Antarctica,
410   Science, 344, 735–738, https://doi.org/10.1126/science.1249055, publisher: American Association for the Advancement of Science, 2014.

Klose, A. K., Wunderling, N., Winkelmann, R., and Donges, J. F.: What do we mean, 'tipping cascade'?, Environmental Research Letters,
16, 125 011, https://doi.org/10.1088/1748-9326/ac3955, publisher: IOP Publishing, 2021.

Klose, A. K., Donges, J. F., Feudel, U., and Winkelmann, R.: Rate-induced tipping cascades arising from interactions between the Greenland
Ice Sheet and the Atlantic Meridional Overturning Circulation, Earth System Dynamics Discussions, pp. 1–25, https://doi.org/10.5194/esd-
415   2023-20, publisher: Copernicus GmbH, 2023.

Lenton, T. M., Held, H., Kriegler, E., Hall, J. W., Lucht, W., Rahmstorf, S., and Schellnhuber, H. J.: Tipping elements in the Earth's cli-
mate system, Proceedings of the National Academy of Sciences, 105, 1786–1793, https://doi.org/10.1073/pnas.0705414105, publisher:
Proceedings of the National Academy of Sciences, 2008.

Lohmann, J. and Ditlevsen, P. D.: Risk of tipping the overturning circulation due to increasing rates of ice melt, Proceedings of the National
420   Academy of Sciences, 118, e2017989 118, https://doi.org/10.1073/pnas.2017989118, publisher: Proceedings of the National Academy of
Sciences, 2021.

Michel, S. L. L., Swingedouw, D., Ortega, P., Gastineau, G., Mignot, J., McCarthy, G., and Khodri, M.: Early warning signal
for a tipping point suggested by a millennial Atlantic Multidecadal Variability reconstruction, Nature Communications, 13, 5176,
https://doi.org/10.1038/s41467-022-32704-3, number: 1 Publisher: Nature Publishing Group, 2022.

425   Morlighem, M., Williams, C. N., Rignot, E., An, L., Arndt, J. E., Bamber, J. L., Catania, G., Chauché, N., Dowdeswell, J. A., Dorschel,
B., Fenty, I., Hogan, K., Howat, I., Hubbard, A., Jakobsson, M., Jordan, T. M., Kjeldsen, K. K., Millan, R., Mayer, L., Mouginot, J.,

Noël, B. P. Y., O'Cofaigh, C., Palmer, S., Rysgaard, S., Seroussi, H., Siegert, M. J., Slabon, P., Straneo, F., van den Broeke, M. R., Weinrebe, W., Wood, M., and Zinglersen, K. B.: BedMachine v3: Complete Bed Topography and Ocean Bathymetry Mapping of Greenland From Multibeam Echo Sounding Combined With Mass Conservation, Geophysical Research Letters, 44, 11,051–11,061, https://doi.org/10.1002/2017GL074954, _eprint: https://onlinelibrary.wiley.com/doi/pdf/10.1002/2017GL074954, 2017.

Morlighem, M., Rignot, E., Binder, T., Blankenship, D., Drews, R., Eagles, G., Eisen, O., Ferraccioli, F., Forsberg, R., Fretwell, P., Goel, V., Greenbaum, J. S., Gudmundsson, H., Guo, J., Helm, V., Hofstede, C., Howat, I., Humbert, A., Jokat, W., Karlsson, N. B., Lee, W. S., Matsuoka, K., Millan, R., Mouginot, J., Paden, J., Pattyn, F., Roberts, J., Rosier, S., Ruppel, A., Seroussi, H., Smith, E. C., Steinhage, D., Sun, B., Broeke, M. R. v. d., Ommen, T. D. v., Wessem, M. v., and Young, D. A.: Deep glacial troughs and stabilizing ridges unveiled beneath the margins of the Antarctic ice sheet, Nature Geoscience, 13, 132–137, https://doi.org/10.1038/s41561-019-0510-8, number: 2 Publisher: Nature Publishing Group, 2020.

Ritchie, P. D. L., Clarke, J. J., Cox, P. M., and Huntingford, C.: Overshooting tipping point thresholds in a changing climate, Nature, 592, 517–523, https://doi.org/10.1038/s41586-021-03263-2, number: 7855 Publisher: Nature Publishing Group, 2021.

Ritchie, P. D. L., Alkhayuon, H., Cox, P. M., and Wieczorek, S.: Rate-induced tipping in natural and human systems, Earth System Dynamics, 14, 669–683, https://doi.org/10.5194/esd-14-669-2023, publisher: Copernicus GmbH, 2023.

Shepherd, A., Ivins, E., Rignot, E., Smith, B., van den Broeke, M., Velicogna, I., Whitehouse, P., Briggs, K., Joughin, I., Krinner, G., Nowicki, S., Payne, T., Scambos, T., Schlegel, N., A, G., Agosta, C., Ahlstrøm, A., Babonis, G., Barletta, V., Blazquez, A., Bonin, J., Csatho, B., Cullather, R., Felikson, D., Fettweis, X., Forsberg, R., Gallee, H., Gardner, A., Gilbert, L., Groh, A., Gunter, B., Hanna, E., Harig, C., Helm, V., Horvath, A., Horwath, M., Khan, S., Kjeldsen, K. K., Konrad, H., Langen, P., Lecavalier, B., Loomis, B., Luthcke, S., McMillan, M., Melini, D., Mernild, S., Mohajerani, Y., Moore, P., Mouginot, J., Moyano, G., Muir, A., Nagler, T., Nield, G., Nilsson, J., Noel, B., Otosaka, I., Pattle, M. E., Peltier, W. R., Pie, N., Rietbroek, R., Rott, H., Sandberg-Sørensen, L., Sasgen, I., Save, H., Scheuchl, B., Schrama, E., Schröder, L., Seo, K.-W., Simonsen, S., Slater, T., Spada, G., Sutterley, T., Talpe, M., Tarasov, L., van de Berg, W. J., van der Wal, W., van Wessem, M., Vishwakarma, B. D., Wiese, D., Wouters, B., and The IMBIE team: Mass balance of the Antarctic Ice Sheet from 1992 to 2017, Nature, 558, 219–222, https://doi.org/10.1038/s41586-018-0179-y, number: 7709 Publisher: Nature Publishing Group, 2018.

Shepherd, A., Ivins, E., Rignot, E., Smith, B., van den Broeke, M., Velicogna, I., Whitehouse, P., Briggs, K., Joughin, I., Krinner, G., Nowicki, S., Payne, T., Scambos, T., Schlegel, N., A, G., Agosta, C., Ahlstrøm, A., Babonis, G., Barletta, V. R., Bjørk, A. A., Blazquez, A., Bonin, J., Colgan, W., Csatho, B., Cullather, R., Engdahl, M. E., Felikson, D., Fettweis, X., Forsberg, R., Hogg, A. E., Gallee, H., Gardner, A., Gilbert, L., Gourmelen, N., Groh, A., Gunter, B., Hanna, E., Harig, C., Helm, V., Horvath, A., Horwath, M., Khan, S., Kjeldsen, K. K., Konrad, H., Langen, P. L., Lecavalier, B., Loomis, B., Luthcke, S., McMillan, M., Melini, D., Mernild, S., Mohajerani, Y., Moore, P., Mottram, R., Mouginot, J., Moyano, G., Muir, A., Nagler, T., Nield, G., Nilsson, J., Noël, B., Otosaka, I., Pattle, M. E., Peltier, W. R., Pie, N., Rietbroek, R., Rott, H., Sandberg Sørensen, L., Sasgen, I., Save, H., Scheuchl, B., Schrama, E., Schröder, L., Seo, K.-W., Simonsen, S. B., Slater, T., Spada, G., Sutterley, T., Talpe, M., Tarasov, L., van de Berg, W. J., van der Wal, W., van Wessem, M., Vishwakarma, B. D., Wiese, D., Wilton, D., Wagner, T., Wouters, B., Wuite, J., and The IMBIE Team: Mass balance of the Greenland Ice Sheet from 1992 to 2018, Nature, 579, 233–239, https://doi.org/10.1038/s41586-019-1855-2, number: 7798 Publisher: Nature Publishing Group, 2020.

Sinet, S.: AMOC Stability Amid Tipping Ice Sheets: The Crucial Role of Rate and Noise [Software], https://doi.org/10.5281/zenodo.10090808, 2023.

Sinet, S., von der Heydt, A. S., and Dijkstra, H. A.: AMOC Stabilization Under the Interaction With Tipping Polar Ice Sheets, Geophysical Research Letters, 50, e2022GL100 305, https://doi.org/10.1029/2022GL100305, _eprint:
465   https://onlinelibrary.wiley.com/doi/pdf/10.1029/2022GL100305, 2023.

Stouffer, R. J., Yin, J., Gregory, J. M., Dixon, K. W., Spelman, M. J., Hurlin, W., Weaver, A. J., Eby, M., Flato, G. M., Hasumi, H., Hu, A., Jungclaus, J. H., Kamenkovich, I. V., Levermann, A., Montoya, M., Murakami, S., Nawrath, S., Oka, A., Peltier, W. R., Robitaille, D. Y., Sokolov, A., Vettoretti, G., and Weber, S. L.: Investigating the Causes of the Response of the Thermohaline Circulation to Past and Future Climate Changes, Journal of Climate, 19, 1365–1387, https://doi.org/10.1175/JCLI3689.1, publisher: American Meteorological Society
470   Section: Journal of Climate, 2006.

Swingedouw, D., Fichefet, T., Goosse, H., and Loutre, M. F.: Impact of transient freshwater releases in the Southern Ocean on the AMOC and climate, Climate Dynamics, 33, 365–381, https://doi.org/10.1007/s00382-008-0496-1, 2009.

Veltz, R.: BifurcationKit.jl, https://hal.archives-ouvertes.fr/hal-02902346, 2020.

Wunderling, N., Donges, J. F., Kurths, J., and Winkelmann, R.: Interacting tipping elements increase risk of climate domino effects under
475   global warming, Earth System Dynamics, 12, 601–619, https://doi.org/10.5194/esd-12-601-2021, 2021.

Wunderling, N., von der Heydt, A., Aksenov, Y., Barker, S., Bastiaansen, R., Brovkin, V., Brunetti, M., Couplet, V., Kleinen, T., Lear, C. H., Lohmann, J., Roman-Cuesta, R. M., Sinet, S., Swingedouw, D., Winkelmann, R., Anand, P., Barichivich, J., Bathiany, S., Baudena, M., Bruun, J. T., Chiessi, C. M., Coxall, H. K., Docquier, D., Donges, J. F., Falkena, S. K. J., Klose, A. K., Obura, D., Rocha, J., Rynders, S., Steinert, N. J., and Willeit, M.: Climate tipping point interactions and cascades: A review, EGUsphere, pp. 1–45,
480   https://doi.org/10.5194/egusphere-2023-1576, publisher: Copernicus GmbH, 2023.